A New Extensional Mixing Element for Improved Dispersive Mixing in Twin-Screw Extrusion, Part 2: Experimental Validation for Immiscible Polymer Blends

SIDNEY O. CARSON, JOÃO M. MAIA

Center for Advanced Polymer Processing, Department of Macromolecular Science and Engineering, Case Western Reserve University, 2100 Adelbert Road, Cleveland, Ohio 44106

JOSÉ A. COVAS

I3N/IPC - Institute for Polymers and Composites, Department of Polymer Engineering, University of Minho 4804-533, Guimarães, Portugal

Correspondence to: João M. Maia, e-mail: joao.maia@case.edu.

ABSTRACT: In Part 1 of this work, we presented a novel static extensional mixing element (EME) for twin-screw extrusion operations and validated the design in terms of the type of flow experienced by the melt upon dispersive mixing. In Part 2, we experimentally demonstrate the ability of the EME to yield improved dispersive mixing when compared with standard kneading-block-induced mixing for immiscible polypropylene/polystyrene blends of varying viscosity ratios between 0.3 and 10. The extensional flow characteristics of the EME improved the dispersion of polystyrene in the blends over all viscosity ratios, with improvements of 30% and above as measured by the cumulative area ratio measurements of polystyrene phases smaller than 1 μm^2. The improvement in dispersive mixing seen from the EME for high viscosity ratio blends opens up applications in other areas, such as dispersion of nanoparticles or in reactive extrusion operations.   © 2016 Wiley Periodicals, Inc. Adv Polym Technol 2016, 0, 21653; View this article online at wileyonlinelibrary.com. DOI 10.1002/adv.21653

KEY WORDS: Blends, Compounding, Extrusion, Mixing, Processing

Introduction

EXTENSIONAL MIXING IN TWIN-SCREW EXTRUSION

Twin-screw extrusion (TSE) is one of the most widely applied operations in the plastics industry for compounding operations (additivation, homogenization, polymer blending, and polymer modification). Some of main advantages of using TSE include adaptability to the different material systems due to construction modularity, encompassment of various individual operation units (melting, secondary solids/liquid feeding, devolatilization, pumping), good control of output and residence time, possibility of direct scaling up from the laboratory to the production level, and high yields. Dispersive mixing action in TSE takes place predominantly through shear flows in screw elements called kneading blocks (KB), whereas distributive mixing is achieved using modified conveying elements. When applied to dispersive mixing (when there is a need to decrease the size of a component), shear flows have been proven to be energetically inefficient when compared to elongational or extensional flows at the same strain.[1,2] Grace[3] showed experimentally that Newtonian–Newtonian emulsions subjected to flows with strong elongational components resulted in finer morphologies and droplet breakup over a wider range of viscosity ratios when compared to shear flows. In fact, when pure shear flows are applied, Grace showed that above a viscosity ratio of approximately 4 it is effectively impossible to continue the droplet breakup process. More practically, the same phenomenon has been studied for non-Newtonian suspensions and was generally proven to show similar effects.[4–6]

The previously mentioned factors for favorable microstructural development were all physical and chemical in nature and solely determined by the properties of the chosen materials. What Grace and others have showed is that materials that are not able to be dispersed and mixed under one type of flow (i.e., shear flows in TSE) have a much greater potential to be mixed under different flow conditions (i.e., extensional flows). The conditions for deformation and breakup of droplets in Grace's studies were quantified as the ratio of the stress exerted on a droplet from the flow and the interfacial stress between the droplet and matrix. This quantity is known as the capillary number and is displayed in Eq. (1):

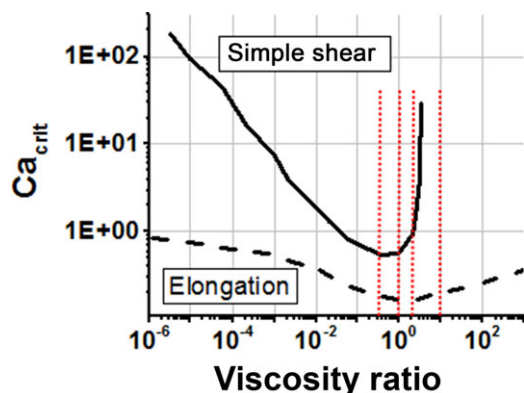$$Ca = \frac{\tau R}{\sigma} \tag{1}$$

FIGURE 1. Critical capillary number necessary to break up Newotnian droplets in a Newtonian matrix for increasing viscosity ratios. Solid line indicates experimental data for simple shear flows, and dashed line indicates elongational flow (adapted from Manas-Zloczower[2] and Grace[3]). Dashed vertical lines represent the viscosity ratios of the blends analyzed in this study. Ratios of 0.3 and 1 correspond to optimal droplet breakup conditions. Viscosity ratios of 3 and 10 correspond to situation of difficult or impossible droplet breakup under pure shear, but not under pure extension.

where τ is the shear stress exerted by the fluid, R is the radius of the droplet, and σ is interfacial tension. The most stable droplet form takes the shape of a sphere, where these stresses are balanced and minimize the surface to volume ratio. Above a certain critical capillary number (Ca_{crit}), the flow stress overtakes the internal, interfacial stresses of the droplet, resulting in the drop being extended and broken up into smaller droplets. Below Ca_{crit}, the drop will only deform under flow. The other critical parameter for droplet breakup that was investigated was the viscosity ratio between the major and dispersed phases of the mixture, defined as

$$\eta_r = \frac{\eta_d}{\eta_m} \qquad (2)$$

where η_d is the viscosity of the dispersed phase and η_m is the viscosity of the major phase. The summary of Grace's experimental results is shown in Fig. 1, which plots the critical capillary number for droplet breakup versus the viscosity ratio for both pure shear and pure extensional flows. Independent of flow type, the minimum Ca_{crit} for droplet breakup is found around a viscosity ratio of 1. However, shear flows were found to be completely ineffective above viscosity ratios of 4, where extensional flows were effective over the entire range of viscosity ratios tested. This and other analyses have driven the development of processing equipment that impose predominantly extensional stresses in operation. These devices have been proven successful in increasing levels of mixing in miscible and immiscible polymer blends[7–9] and polymeric nanocomposites.[10,11] However, the practical application of extension dominated flow using these devices is still incomplete from a scale and ease of application standpoint.

In Part 1 of this work, we presented[12] and validated from the non-Newtonian fluid mechanics perspective a new concept of extensional mixing element (EME) for TSE operations. It differed from the previously discussed extensional mixing devices[4,7–11,13,14] in that it is built into the established construction of the TSE without adding any peripheral equipment systems, though efforts have been made to impart extension dominated flow within a TSE's barrel.[15–18] The EME is a static screw element of a TSE that provided mixing by forcing material through hyperbolically contracting–diverging flow channels inside the extruder barrel. As mentioned in Part 1,[12] these hyperbolic channels impart a uniform predetermined extension rate along their centerline, which can be calculated nominally[19] from the flow rate through the channel as well as the channel dimensions. The EME was designed to increase the dispersive mixing capabilities of a TSE system, since distributive mixing is more easily achieved with current screw element designs. The computational validation of the EME concluded that the desired extensional characteristics were present in all of the flow channels, which was confirmed by the velocity profiles (linearly increasing along the centerlines) and the stress states under real-operating conditions (normal stresses in the flow direction being greater in magnitude when compared to shear stresses). Overall, Part 1 proved that (1) a static screw element inside the barrel of a TSE is a viable construction, (2) the performance of such an element can be predicted accurately through computational flow analysis, and (3) the implementation of hyperbolic flow channels on a TSE element imparts extension dominated flow based on the velocity profiles and stress states.

Part 2 of this discussion will investigate the real experimental performance of the EME, where we study the dispersion states of incompatible, matched, and mismatched viscosity polypropylene/polystyrene (PP/PS) blends. The resulting blend morphologies are compared to the morphologies obtained through a traditional, highly restrictive KB configuration, which is the current standard for TSE mixing and shown to be finer and to develop faster, including for very high viscosity ratios.

Experimental

PROCESSING EQUIPMENT

The TSE used for the experiments was a ThermoScientific, Waltham, MA, US TSE24MC 24-mm corotating twin-screw extruder with a 40:1 L/D ratio. The TSE24MC extruder was specially constructed to have 14 movable pressure/temperature (P/T) transducer ports along the length of the barrel. The layout of these ports is shown in Fig. 2.

The two screw configurations used for all studies are shown in Fig. 3. These configurations were designed to be identical other than the single mixing zone. The "KB" configuration included 3.25 L/D of 90° KB elements at this location. This KB geometry is neutral from the conveying point-of-view and therefore directly comparable with the EME, which is also nonconveying. The "EME" configuration included the EME as well as 90° KB elements before and after, with the total length of the mixing section equaling 3.25 L/D as well. The KB elements before and after the EME were placed there to keep the total length of the mixing sections equal and also due to the EME being designed to interface with the KB (instead of conveying) elements.
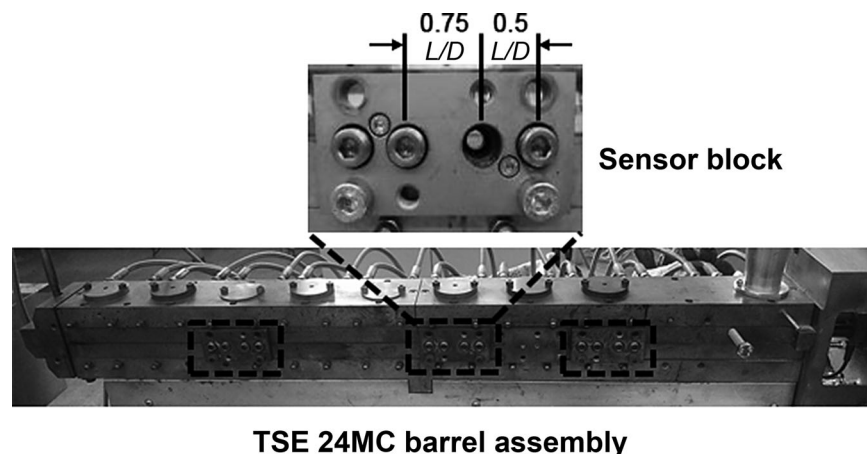
TSE 24MC barrel assembly

FIGURE 2. Sensor port arrangement for the barrel of the twin-screw extruder used in this study.
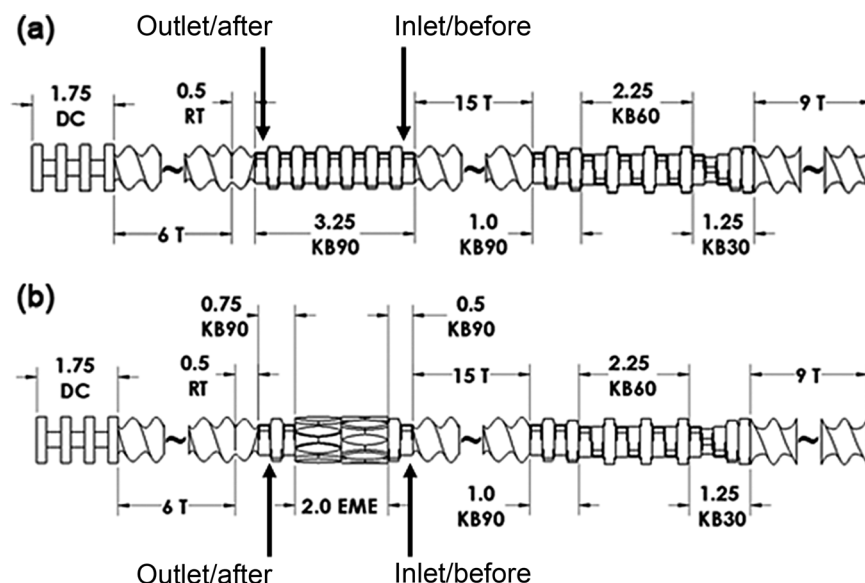

FIGURE 3. Screw configurations for all experimental trials. (a) 90° "KB" configuration and (b) "EME" configuration. Relevant measurement and sampling locations are indicated.

Both configurations have a reverse conveying element placed at the exit of the described mixing sections to promote and maintain distributive mixing characteristics after the EME, to guarantee the EME channels are filled, and to guarantee enough pressure is present in the system to collect samples at the outlet (as described later). It was included in the KB geometry to make the mixing section as restrictive as possible.

Screw rotation speed was set to a constant 500 rpm for all experiments. Material was fed into the extruder at a constant rate of 5.5 kg/h for all experiments using a Brabender volumetric feeder with a single spiral screw configuration. Material was extruded through a three-hole strand die with a hole diameter of 3 mm and collected through a ThermoScientific water bath and pelletizer. Pressure measurements were taken before and after the mixing zones (as indicated in Fig. 3) using Dynisco, Franklin, MA, US MDA422 transducers connected to a Dynisco 1390 instrumentation box. Temperature measurements were taken at

the same locations using Pyromation, Fort Wayne, IN, US JMM-B23U transducers connected a Fluke, Everett, WA, US 52 II thermometer. These transducers were flush mounted to the extruder screws. Temperature readings were taken in process for all of the neat PP resins, and the reported values are shown as averages between the inlet and outlet temperatures (again, as indicated in Fig. 3). These pressure and temperature readings were taken after allowing the process to stabilize for approximately 15 min. All process characteristic measurements were taken in triplicate, after stopping the process and allowing it to return to a quiescent state.

The "sample collector" (SC), shown in Fig. 4, was developed as part of an effort to characterize material development in-process along the axis of an extruder. Online measurement techniques have been implemented previously to study the evolution of blend morphologies, chemical reactions, and dispersion processes.[20–26] The SC was meant as a more universal device that
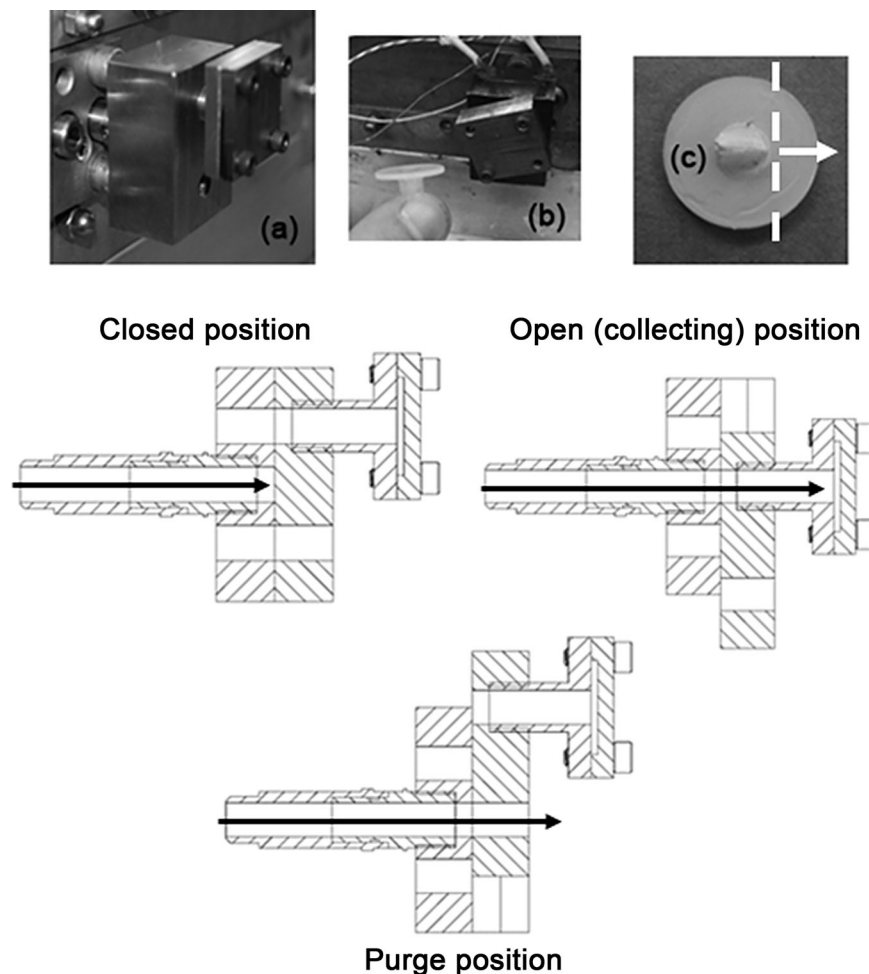
FIGURE 4. (a) The SC, attached to a *P/T* port of a TSE. (b) The SC attached with collected sample shown. (c) Final disk with cross-sectional face indicated. (d) Cross-sectional view of the SC in operation. Material flow is transverse to the extrusion direction and is indicated by arrows. Three positions are closed during normal operation, purge to clear collection channel, and collection for flow into mold.

would interface with any standard *P/T* port present on a commercial extruder. The SC acts as a three-position on/off valve for the collection of material out of a *P/T* port, with the ability to mold a sample of any geometry (a disk in this case) directly out of the extruder. One limitation of current online sampling methods is the necessity of reforming the sample after quenching into a useful form, and the SC avoids that by directly molding samples. Figure 4d shows the different operating positions of the SC: (i) the "closed" position, where no material is flowing out, creating a plug inside the device; (ii) the "purge" position, which is used before collecting to clear the plug out of the device, ensuring fresh material is used for the collected sample; (iii) the "open" position, where material flows directly into the mold, or out of the device. Total time taken to collect a sample from the SC is less than 1 min, from the start of the purge cycle, where the material is allowed to completely clear out, to the end of the collection cycle, where the mold and sample are removed and allowed to cool. Each sample diverts approximately 15–20 g of material, depending on the amount of time the device is allowed to purge, so the main flow in the extruder is not disturbed.

Samples were taken during compounding of all blends with both screw configurations at the "after" position indicated in Fig. 3. Three samples of each composition and screw configuration combination were taken.

RHEOLOGICAL CHARACTERIZATION

Three PS and three PP materials were thermorheologically characterized for this study. These were named PS1–3 and PP1–3 for the purposes of these experiments. Shear measurements were performed using a TA Instruments, New Castle, DE, US ARES G2 rotational rheometer equipped with a 25-mm parallel plate geometry enclosed in an environmental chamber for temperature control. Small amplitude oscillatory shear frequency sweeps were conducted using a strain of 1% at angular frequencies ranging from 0.1 to 100 rad/s for each test. Shear properties were tested at a range of 200–300°C in 10°C increments. The complex viscosity (η^*) at a given frequency obtained from these tests was assumed to be equal to the steady shear viscosity (η) at an equivalent shear rate, as stated by the Cox–Merz relation.[27] Each of the

polymers tested in this study was homopolymers with simple flow and relaxation behavior, and therefore the principles of Cox–Merz were assumed to hold. Time-temperature superposition (TTS) for the shear viscosity was performed using the IRIS Rheo-Hub software. Material samples for rheological measurements were compression molded at 230°C on a compression molder for 4 min under an applied load of 8 metric tons. Samples for shear were 25-mm diameter × 1-mm thick disks. Each material was modeled as a generalized Newtonian fluid with a shear-rate-dependent viscosity governed by the Cross law, which is defined as

$$\eta(\dot{\gamma}) = \frac{\eta_0}{1 + (\lambda\dot{\gamma})^{1-n}} \tag{3}$$

where n is the power law index, η_0 is the zero shear rate viscosity, and λ is the natural time, defined as the inverse of the shear rate where the fluid begins to shear thin.

Four different blends were chosen as model systems to investigate, differentiated by their effective viscosity ratios, as explained later. The blends were all of 80/20 PP/PS wt% and were premixed in 2.2-kg batches before being introduced to the extruder feeder. In all cases, the dispersed phase represents the PS and the major phase the PP.

MORPHOLOGICAL ANALYSIS

All blends were characterized using scanning electron microscopy on a JEOL, Akishima, Tokyo, Japan JSM-6510LV scanning electron microscope (SEM) using a 30-kV beam voltage. Disk samples taken from the SC were cut and prepared as indicated in Fig. 4c. The disks were first punched out and cut to a proper size for the SEM stages. The cross-sectioned surface of each sample was cryo-microtomed at −30°C using a glass knife on a Leica, Wetzlar, Germany EM UC6 microtome, using a cutting speed and thickness of 2 mm/s and 1 μm, respectively. Each sample was soaked in tetrahydrofuran (THF) for 18 h to extract the PS phase from the blend to observe contrast. The samples were coated with gold at a thickness of 5 nm with an EMS Quorum sputter coater. The size and shape of PS phases were analyzed using ImageJ.

While visible inspection was sufficient to observe general patterns, dispersion, and distribution levels, a more quantifiable method was desired to observe the relative performance of the EME and KB screw configurations. However, since the PS domain size distributions seen in all samples are highly nonuniform, with a combination of spherical and nonspherical droplet phases being observed, taking the average size of the PS domains would not yield useful information. Instead, the variation of the cumulative PS domain area ratio distribution was observed with respect to the PS domain area. Although different global dispersion indicators could have been used, we believe this effectively represents the differences in dispersive mixing ability between the two screw configurations. The cumulative area ratio distribution was calculated by[28]

$$F_{[i,j]} (\%) = \left(\frac{\sum_{i=j} A_{[i,j]}}{\sum_{i=j} A_n} \right) \tag{4}$$

where $A_{[i,j]}$ represents the area of the PS domain that has been ranked from the smallest to the jth domain, and A_n represents the total PS domain area. These values were then plotted against domain area A_i. In this way, the shape and asymmetrical size distribution of the measure agglomerate is accounted for in the statistical analysis, giving a more direct measure of the dispersive mixing capability of the two mixers. Approximately, 200 PS domains from different locations on the sample were measured for each composition and screw configuration.

Results and Discussion

DETERMINING EFFECTIVE VISCOSITY RATIOS

The goal of this study was to compound simple, incompatible blends of differing viscosity ratios through both the KB and EME screw configurations and compare their resulting morphologies. Four different effective viscosity ratios were chosen for analysis: 0.3, 1, 3, and 10. These ratios correspond to important viscosity ratios in Grace's analysis of droplet breakup, as shown in Fig. 1.[3] Viscosity ratios of 0.3 and 1 correspond to the region of optimal droplet breakup (where the magnitude of the Ca necessary to break up droplets is the lowest). As the viscosity ratio approaches 3, shear becomes progressively more ineffective at breaking up droplets (which becomes an impossibility in shear flows at $\eta_r > 4$). At a viscosity ratio of 10, it is theoretically predicted that a simple shear flow will not be able to break up the disperse phase droplets. Even though flow in the KBs is shear dominated, there is a significant extensional component due to the squeezing motion of the elements against the barrel walls, in the intermeshing zone between individual elements, and possibly in the opposing flow created by the reverse conveying element after the mixing section. Therefore, we expect the conventional KB screw configuration to still be able to provide droplet breakup at high viscosity ratios, but also that the EME configuration will be more efficient at doing so.

To obtain the effective viscosity ratio of a given blend, consideration was made to both the approximate temperature (which will differ from the extruder set point due to viscous heating) and shear rate (which can be calculated computationally) inside the mixing sections during processing. This guarantees that the viscosity ratios inside the extruder, during mixing, are the effective ones and not nominal values.

Table I shows the results of the temperature studies, which are displayed as averages between the measured inlet and outlet (indicated in Fig. 3) temperatures during processing of all of the neat PP resins at increasing barrel temperatures. It was concluded that PP1 showed approximate temperature rises ranging from 10 to 20°C, PP2 from 15 to 30°C, and PP3 from 7 to 18°C, independently of whether KBs or EMEs being used. These values were used as a guideline for choosing the approximate real temperature of mixing according to the set barrel temperature and the base PP resin being used in a given blend. Following this analysis, each material was fitted to the Cross law at each tested temperature and at shear rates between 0.001 and 1000 s^{-1}.

TABLE I ▪
Temperature Rise in Mixing Sections for KB and EME Configurations

	ΔT KB	+/−	ΔT KB	+/−	ΔT KB	+/−
PP1	19.8	3.3	16.8	2.3	10.5	1.0
PP2	27.8	5.8	22.0	2.5	14.5	1.0
PP3	13.0	5.0	14.0	2.0	8.0	1.5
	ΔT EME	+/−	ΔT EME	+/−	ΔT EME	+/−
PP1	15.5	1.5	11.5	2.5	7.8	1.8
PP2	18.8	0.8	15.5	5.5	12.3	2.3
PP3	8.3	3.3	8.0	5.0	4.8	3.8
	Set = 200		Set = 220		Set = 240	

TABLE II ▪
Real Viscosity Ratios Calculated as a Function of Shear Rate for All of the Chosen Blends

Shear Rate	PS1/PP2	PS3/PP2	PS1/PP3	PS3/PP3
32	0.2	1.0	2.6	11.6
40	0.3	1.0	2.7	11.4
50	0.3	1.0	2.8	11.1
63	0.3	1.0	3.0	10.9
79	0.3	1.0	3.1	10.6
100	0.3	1.0	3.2	10.4
126	0.3	1.0	3.3	10.1
158	0.3	1.0	3.4	9.9
199	0.4	0.9	3.5	9.6

In this way, viscosity data at all processing temperatures over a wide range of shear rates were determined for all potential material pairs.

Complex viscosity versus frequency curves for the chosen blends are shown in Fig. 5. The areas of the processing window are highlighted between 30 and 200 s^{-1}. These shear rates were chosen based on the minimum and maximum shear rates present in the flow channels in the EME, described in Part 1 of this work. To determine the viscosity ratios, Eq. (2) was applied to the viscosity values in the processing window, and these are shown in Table II. All viscosity ratios displayed in Table II were calculated for the temperature of the barrel plus the ΔT calculated for the PP resin in Table I. As can be seen, the effective viscosity ratios of the selected material pairs are very close to the nominal values at all shear rates.

This elaborate procedure to calculate the effective viscosity ratios under the real thermomechanical processing conditions

was critical because Grace's analysis of droplet breakup was conducted for Newtonian droplets in a Newtonian matrix; therefore, it was important that the effective viscosity ratios were as independent of shear rate as possible. For the $\eta_r = 1$ blends, PS3 and PP2 were chosen, and the viscosity ratios were equal to 1.0 and almost completely independent of shear rate. For $\eta_r = 10$, PS3 and PP3 were chosen, and the viscosity ratio dropped as the shear rate increased, but still averaged at 10.6 ± 0.7, which is quite acceptable. Both of these blends were processed at a barrel temperature of 200°C. For both $\eta_r = 3$ (PS1 and PP3) and $\eta_r = 0.3$ (PS1 and PP2), the viscosity ratios increased slightly with the shear rate, but again averaged to near the desired values at 3.1 ± 0.3 and 0.3 ± 0.1, respectively. These blends were processed at a barrel temperature of 240°C.
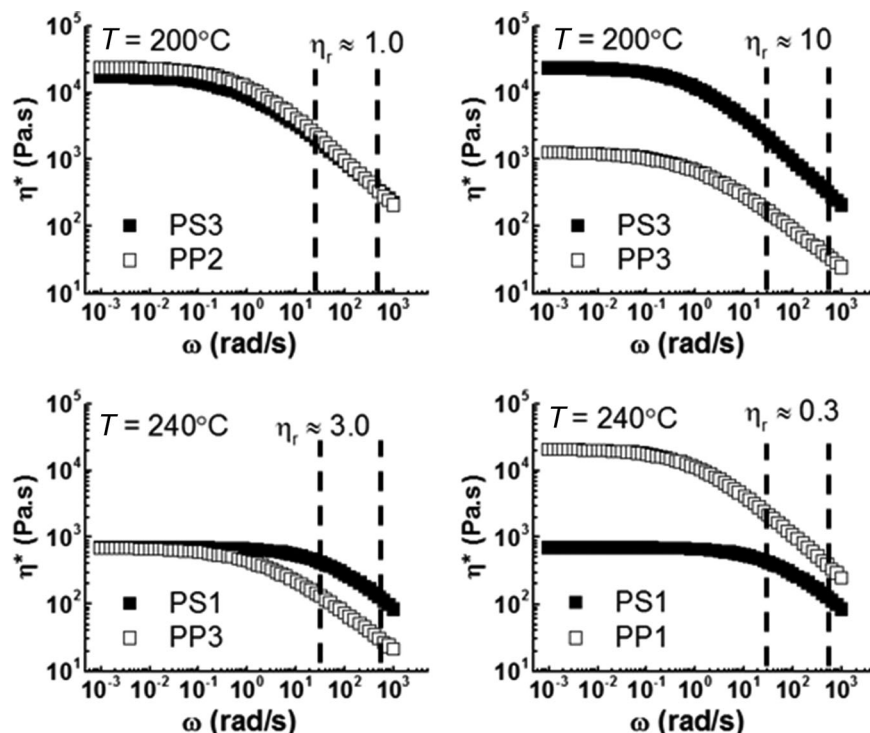

FIGURE 5. Complex viscosity measurements at chosen processing temperatures for all blends, with processing shear rates highlighted.

Pressure Profiles for All Blends Compounded through Both Screw Configurations

|	KB			EME		
Viscosity Ratio	Outlet Pressure (bar)	Inlet Pressure (bar)	ΔP (bar)	Outlet Pressure (bar)	Inlet Pressure (bar)	ΔP (bar)
≈ 0.3	100	120	20	100	280	180
≈ 1.0	100	110	10	80	210	130
≈ 3.0	60	70	10	80	160	80
≈ 10	80	85	5	75	185	110

PRESSURE PROFILES

The inlet pressure, outlet pressure, and pressure drop measurements for all blends compounded through both the KB and EME screw configurations are shown in Table III. All EME configuration processes showed pressure drops of around one order of magnitude more when compared to the same processes using the KB configuration. The pressure drop across a mixing zone can provide an indirect measure of the overall stress levels in the system during compounding. This is a first indication that dispersive mixing across the different mixing geometries would be improved using the EME, since dispersive mixing is stress dependent. Another consequence of the pressure differences between the mixing geometries could be an increased motor load on the extruder: The average load was 0.40 kWh for all of the KB blends and 0.43 kWh for all of the EME blends. These values are very similar, even given the large pressure profile difference for each screw configuration, because the differences in pressure arise in a small axial length and both of the mixing geometries are conveying neutral. Therefore, the EME was concluded to not significantly affect the power consumption of the process.

BLEND MORPHOLOGY

The SEM micrographs of all of the blends at the end of the respective mixing sections for both screw configurations are shown in Fig. 6. Each image is shown as a representative sample of each composition and screw configuration. The dark droplet areas represent the extracted PS phases. In general, the EME configuration improved the dispersion and distribution of the PS over the KB configuration across all viscosity ratios. The most visible improvement was shown in the blend with $\eta_r = 3$, which resulted in a very uniform droplet size and shape from the EME, compared to very elongated and uneven phases from the KB. Blends with $\eta_r = 0.3$ and $\eta_r = 1$ also showed noticeable improvement, with an overall smaller apparent droplet size and less elongated phases in the EME, even though these blends have the ideal viscosity ratio for droplet breakup in shear. The $\eta_r = 10$ blend also showed significant improvement, with the EME configuration yielding a mix of highly elongated droplets and small droplets already broken-up and the KB configuration showing almost elongated droplets only, with little or no small droplets.

The cumulative area ratio plots are shown in Fig. 7. For all of these plots, the percentage of PS domains under 1 μm^2 was chosen as the metric to compare the dispersive mixing efficiencies of the screw configurations. The vertical dashed line represents
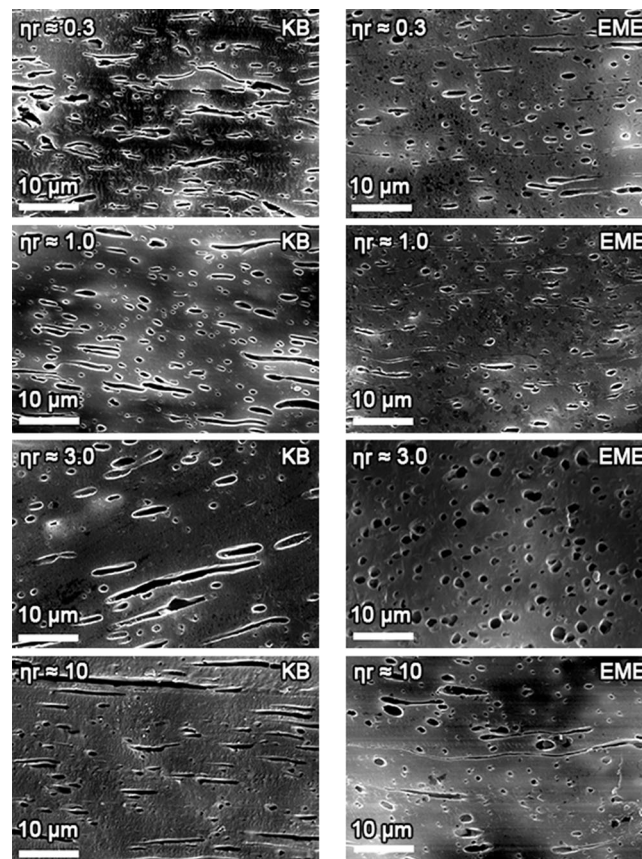
FIGURE 6. SEM micrographs of blend morphologies for all blends. Left column shows KB results; right column shows EME results.

Cumulative PS Domain Area Ratio Distribution and Maximum PS Domain Measurements for All Blends

	% of Domains w/Area < 1 μm^2			
	$\eta_r \approx 0.3$	$\eta_r \approx 1$	$\eta_r \approx 3$	$\eta_r \approx 10$
KB	50	42	21	22
EME	61	75	45	41
Δ (%)	+22	+79	+114	+86
	Maximum Domain Area (μm^2)			
	$\eta_r \approx 0.3$	$\eta_r \approx 1$	$\eta_r \approx 3$	$\eta_r \approx 10$
KB	4.3	5.3	5.0	5.9
EME	4.4	2.5	3.9	5.5
Δ (%)	+2	−53	−22	−7

this cutoff, where an increased slope between data sets indicates a better dispersed system (more domains under 1 μm^2). These values along with the maximum measured PS domain area (taken from the representative images in Fig. 6) are displayed in Table IV. For the KB configuration, blends with $\eta_r = 0.3$ and $\eta_r = 1$ showed comparable dispersion, while the $\eta_r = 3$ and $\eta_r = 10$ blends showed poorly dispersed morphologies. These numbers confirm the visual inspections of the samples. The EME improved the dispersion numbers for all viscosity ratios. For $\eta_r = 0.3$, the percentage of domains with areas smaller than
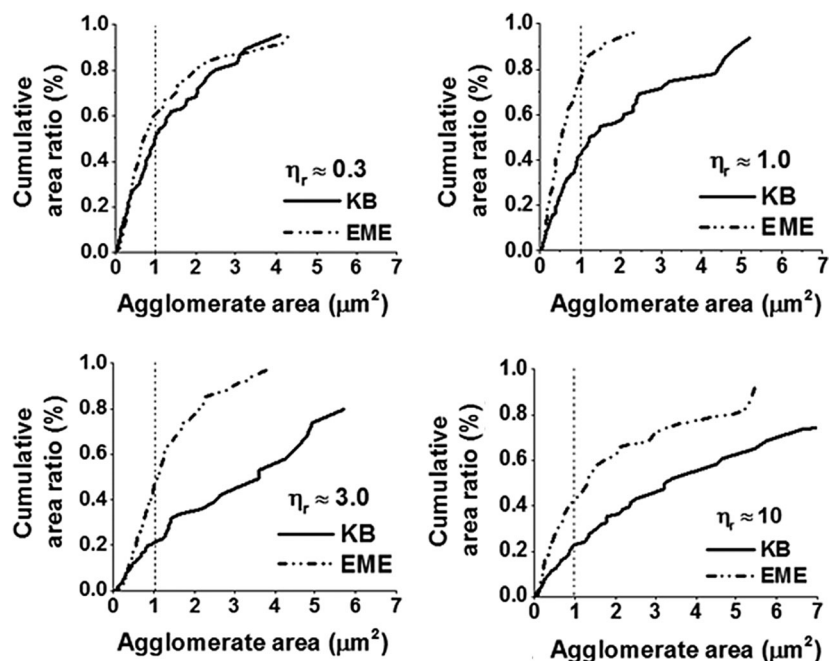
FIGURE 7. Cumulative area ratio distribution measurements for all blends at all screw configurations. Dashed line at 1 μm^2 for the agglomerate area represents the chosen cutoff for dispersion effectiveness.

1 μm^2 increased by 22% with the EME, whereas the maximum domain size remained unchanged. For the other samples, the percentage of domains with areas smaller than 1 μm^2 was always higher than approximately 80% and maximum domain size decreased by as much as 50%. This is an important result since it confirms the ineffectiveness of shear and effectiveness of elongation at dispersing high viscosity ratio samples.

Conclusions

The EME was previously developed as a screw element for TSE that imparts extension-dominated flow on a compounded material. Since shear flows (which are the predominant forces in current TSE technology) are energetically inefficient in dispersion processes when compared to elognational flows, we compared the effectiveness of a standard TSE screw to an EME configuration in dispersing simple polymer blend systems with increasing viscosity ratios. Incompatible 80/20 wt% PP/PS blends of viscosity ratios of 0.3, 1, 3, and 10 were compounded using two screw configurations: the first with a standard KB mixing section and the second with the experimental EME in place of the KB. Samples at the end of the mixing sections of each screw were collected using the SC, developed as a method for characterizing materials online along the axis of the extruder. These samples were immediately molded into a disk geometry without the need for remelting. The cross section of these disks was then investigated using SEM after extracting the PS phase using THF, and the areas of the extracted domains were measured and ranked against each other using a cumulative area ratio distribution measurement.

Visual inspections of the blends showed that the EME samples had a generally better dispersed PS morphology over all the viscosity ratios when compared to the KB samples. In previous studies of droplet deformation under flow, it was observed that above a threshold viscosity ratio, droplets under shear will elongate almost indefinitely without breaking.[2,3,5,6,29] In the analysis of the blend morphology, we observed extremely elongated PS phases to be more prevalent in the KB configuration samples and greatly reduced in the EME samples that, in turn, showed smaller droplet size. The cumulative area ratio distribution measurements showed significant improvements in the dispersion levels for all viscosity ratios. The important conclusions to be taken out of these results are (1) the EME was successful in effectively dispersing immiscible polymer blends of varying viscosity ratios under real extrusion conditions and (2) the comparison of the KB and EME configurations confirmed previous analyses of droplet breakup effectiveness under shear and elongation, only on a larger and more applied scale. In the future, more opportunity exists for the study of dispersion of nanoparticles, such as carbon nanotubes or nanoclays, or some reactive extrusion operations. These systems often cannot be processed effectively through traditional TSE alone, and the application of the EME in those areas could provide technical advances and further validation of the device.

Acknowledgments

▌ References

1. Erwin, L. In Mixing in Polymer Processing; Marcel Dekker: new York, 1991; pp. 1–16.

2. Manas-Zloczower, I. Mixing and Compounding of Polymers: Theory and Practice; Hanser: Cincinnati, OH, 2009.

3. Grace, H. P. Chem Eng Commun 1982, 14, 225–277.

4. Bourry, D.; Godbille, F.; Khayat, R. E.; Luciani, A.; Picot, J.; Utracki, L. A. Polym Eng Sci 1999, 39, 1072–1086.

5. Guido, S. Curr Opin Colloid Interface Sci 2011, 16, 61–70.

6. Milliken, W. J.; Leal, L. G. J Non-Newtonian Fluid Mech 1991, 40, 355–379.

7. Bouquey, M.; Loux, C.; Muller, R.; Bouchet, G. J Appl Polym Sci 2011, 119, 482–490.

8. Luciani, A.; Utracki, L. A. Int Polym Process 1996, 11, 299–309.

9. Rondin, J.; Bouquey, M.; Muller, R.; Serra, C. A.; Martin, G.; Sonntag, P. Polym Eng Sci 2014, 54, 1444–1457.

10. Ibarra-Gómez, R.; Muller, R.; Bouquey, M.; Rondin, J.; Serra, C. A.; Hassouna, F.; Mouedden, Y. E.; Toniazzo, V.; Ruch, D. Polym Eng Sci 2015, 55, 214–222.

11. Tokihisa, M.; Yakemoto, K.; Sakai, T.; Utracki, L. A.; Sepehr, M.; Li, J.; Simard, Y. Polym Eng Sci 2006, 46, 1040–1050.

12. Carson, S. O.; Covas, J. A.; Maia, J. M. Advances in Polymer Technology, 2015.

13. Khayat, R. E.; Luciani, A.; Utracki, L. A.; Godbille, F.; Picot, J. Int J Multiphase Flow 2000, 26, 17–44.

14. Nguyen, X. Q.; Utracki, L. A. United States Patent 5451106, 1995.

15. Wang, N.; Sakai, T.; Hashimoto, N. Int Polym Process 1998, 13, 27–32.

16. Jacobsen, S.; Fritz, H.; Degée, P.; Dubois, P.; Jérôme, R. Polymer 2000, 41, 3395–3403.

17. Garcia, M.; van Vliet, G.; Jain, S.; Schrauwen, B.; Sarkissov, A.; van Zyl, W.; Boukamp, B. Rev Adv Mater Sci 2004, 6, 169–175.

18. Kohlgrüber, K. Co-Rotating Twin-Screw Extruder; Carl Hanser: Munich, Germany, 2012.

19. Ober, T. J.; Haward, S. J.; Pipe, C. J.; Soulages, J.; McKinley, G. H. Rheol Acta 2013, 52, 529–546.

20. Cho, S.; Hong, J. S.; Lee, S. J.; Ahn, K. H.; Covas, J. A.; Maia, J. M. Macromol Mater Eng 2011, 296, 341–348.

21. Covas, J. A.; Carneiro, O. S.; Costa, P.; Machado, A. V.; Maia, J. M. Plast, Rubber Compos 2004, 33, 55–61.

22. Covas, J. A.; Carneiro, O. S.; Maia, J. M.; Filipe, S. A.; Machado, A. V. Can J Chem Eng 2002, 80, 1065–1074.

23. Covas, J. A.; Maia, J. M.; Machado, A. V.; Costa, P. J Non-Newtonian Fluid Mech 2008, 148, 88–96.

24. Covas, J. A.; Nobrega, J. M.; Maia, J. M. Polym Test 2000, 19, 165–176.

25. Filipe, S.; Cidade, M. T.; Wilhelm, M.; Maia, J. M. Polymer 2004, 45, 2367–2380.

26. Machado, A. V.; Maia, J. M.; Canevarolo, S. V.; Covas, J. A. J Appl Polym Sci 2004, 91, 2711–2720.

27. Cox, W.; Merz, E. J Polym Sci 1958, 28, 619–622.

28. Jamali, S.; Paiva, M. C.; Covas, J. A. Polym Test 2013, 32, 701–707.

29. Bentley, B. J.; Leal, L. G. J Fluid Mech 1986, 167, 241–283.